AN ABSTRACT OF THE CAPSTONE REPORT OF

Trisha Kishore Bhagde for the degree of Master of Chemical Sciences

Title: Electronic Spectroscopy of Methacrolein Oxide:
A Four Carbon Criegee Intermediate from Isoprene Ozonolysis

Project conducted at: University of Pennsylvania
Department of Chemistry
231 S 34th Street
Philadelphia PA 19104
Supervisor: Prof. Marsha I. Lester
Dates of Project: May 1, 2018- May 19, 2019

Abstract approved:

Marsha I. Lester, Academic Advisor

Abstract

Isoprene is an unsaturated hydrocarbon and the most abundant non-methane hydrocarbon in Earth's atmosphere. Atmospheric oxidation of isoprene via reaction with ozone leads to formation of carbonyl oxide intermediates, known as Criegee intermediates. Methacrolein oxide (MACR-oxide, $(CH_2=C(CH_3))CHOO$), is a four carbon unsaturated Criegee intermediate produced in isoprene ozonolysis. The aim of this study is to obtain the UV-Visible absorption spectrum of MACR-oxide on a strong $\pi^*\leftarrow\pi$ electronic transition associated with the conjugated carbonyl oxide and vinyl groups. MACR-oxide is synthesized in the laboratory by photolyzing a diiodo alkene precursor (1,3-diiodo-2-methylprop-1-ene) followed by reaction with oxygen that transiently forms a iodoalkene peroxy radical. Subsequent loss an iodine atom yields MACR-oxide in four conformational forms. MACR-oxide is produced in a quartz capillary reactor tube and cooled in a pulsed supersonic jet expansion. MACR-oxide is detected by photoionization using 118 nm VUV radiation on the m/z = 86 mass channel of a time of flight mass spectrometer. UV-Visible radiation is absorbed and promotes MACR-oxide from its ground state to an excited $1^1\pi\pi^*$ electronic state. This results in a ground state depletion that is detected as a reduction in the 118 nm photoionization signal. The UV-Visible spectrum of MACR-oxide is observed from 315 to 500 nm and peaks at 380 nm. Weak oscillatory structure is found in the long wavelength region of the spectrum, which can be attributed to vibrational resonances. Complementary Velocity Map Imaging experiments show that MACR-oxide dissociates rapidly upon UV-Visible excitation. This assures that the UV-Visible spectrum of MACR-oxide obtained by the depletion method is equivalent to a direct absorption measurement. The UV-visible spectrum of MACR-oxide is expected to have broad applicability as a sensitive probe of its unimolecular decay and bimolecular reactions with trace species relevant in the atmosphere.

Electronic Spectroscopy and photochemistry of Methacrolein Oxide: A Four Carbon Criegee Intermediate from Isoprene Ozonolysis

by

Trisha Kishore Bhagde

A CAPSTONE REPORT

submitted to the

University of Pennsylvania

in partial fulfillment of
the requirements for
the degree of

Master of Chemical Sciences

Presented: April 9, 2019
Commencement: May 19, 2019

Master of Chemical Sciences Capstone Report of Trisha Kishore Bhagde presented on April 9, 2019.

APPROVED:

Marsha I. Lester, representing Physical Chemistry

I understand that my Capstone Report will become part of the permanent collection of the University of Pennsylvania Master of Chemical Sciences Program. My signature below authorizes release of my final report to any reader upon request.

Trisha Kishore Bhagde, Author

Acknowledgements

I would like to thank Prof. Marsha I. Lester for her guidance throughout this capstone and allowing me to work in her laboratory. I would like to express my gratitude to Prof. Jessica Anna and Dr. Ana-Rita Mayol-Cabassa for their support and guidance throughout this process of acquiring my MCS degree and the completion of my Capstone. I am also very appreciative of the help I have received by the staff at the Department of Chemistry. I would like to thank the members of the Lester group for their support and for extending their knowledge to me. This Capstone would not have been possible without them.

Table of Contents

List of Figures

List of Tables

List of Schemes

List of Appendices

Introduction

Volatile Organic Compounds (VOC) in the atmosphere originate from biogenic, anthropogenic and oceanic sources. On a global scale, the generation of VOC's from biogenic sources exceed that from anthropogenic sources. However, in urban environments, the opposite holds true.[1] Anthropogenic sources include combustion processes, use of fossil fuels, industrial processes and, solvents. VOCs from biogenic sources include isoprene and α-pinene which play an important role in atmospheric reactions.[2]

Isoprene, **1**, is the most abundant VOC in the atmosphere after methane. Isoprene is mostly emitted from different kinds of trees and shrubs. These include oaks, poplars, eucalyptus and some legumes.[3] Recent studies estimate a global isoprene emission of nearly 600 Tg per annum and accounts for almost one- third of the total hydrocarbons emitted in the atmosphere.[4]

Alkenes have different removal pathways from the atmosphere. Alkenes are known to be very reactive with hydroxyl radicals (OH), ozone (O_3) and nitrate radicals (NO_3) (primarily in the nighttime).[5] Alkenes are more reactive with hydroxyl radicals than with ozone. However, the abundance of ozone in the atmosphere is larger than that of hydroxyl radicals, making the reaction pathway of alkenes, including isoprene, with ozone an important focus of study.[6–8]

Isoprene **1** is the most abundant alkene in the atmosphere and can produce three different Criegee intermediates *via* ozonolysis. **Scheme 1**[9] shows the mechanism of isoprene ozonolysis. Isoprene **1** has two carbon-carbon double bonds. When ozone adds to the $C_{(3)}$-$C_{(4)}$ double bond of **1**, it forms a primary ozonide (POZ) **2**, which subsequently breaks apart to form methacrolein oxide (MACR-oxide, (CH_2=C(CH_3))CHOO) **3**, a four carbon unsaturated Criegee intermediate, and formaldehyde **4**, or it could form the simplest Criegee intermediate, CH_2OO **5**, and methacrolein **6**. Alternately, if the ozone adds to the $C_{(1)}$-$C_{(2)}$ double bond of isoprene **1**, then it forms an isomeric form of POZ **7**, which leads to the formation of methyl vinyl ketone oxide (MVK-oxide, $CH_2CHC(CH_3)OO$) **8** and formaldehyde **4**, or CH_2OO **5** and methyl vinyl ketone **9**.[10,11] MACR-oxide **3**, MVK-oxide **8** and CH_2OO **5** contain carbonyl oxide groups that are zwitterionic in nature. MACR-oxide **3** and MVK-oxide **8** are structural isomers.[12–15] Hence, two four-carbon unsaturated Criegee intermediates, MVK-oxide **8** and MACR-oxide **3**, are formed depending on whether ozone adds across the carbon-carbon double bond with or without the methyl substitution, respectively. Prior studies estimate that MACR-oxide **3** and MVK-oxide **8** account for approximately 19% and 23% of the Criegee intermediates formed in isoprene ozonolysis, respectively.[12,16] Criegee intermediates are a significant source of OH radicals, particularly under low light conditions and are also known to react with a variety of atmospheric species (H_2O, SO_2, etc.).[17–20]

Scheme 1. Ozonolysis of isoprene 1 to form MACR-oxide 3, CH_2OO 5, MVK-oxide 8, and their respective carbonyl compounds formaldehyde 4, methacrolein 6, and methyl vinyl ketone 9, via the POZ 2, 7 pathway.

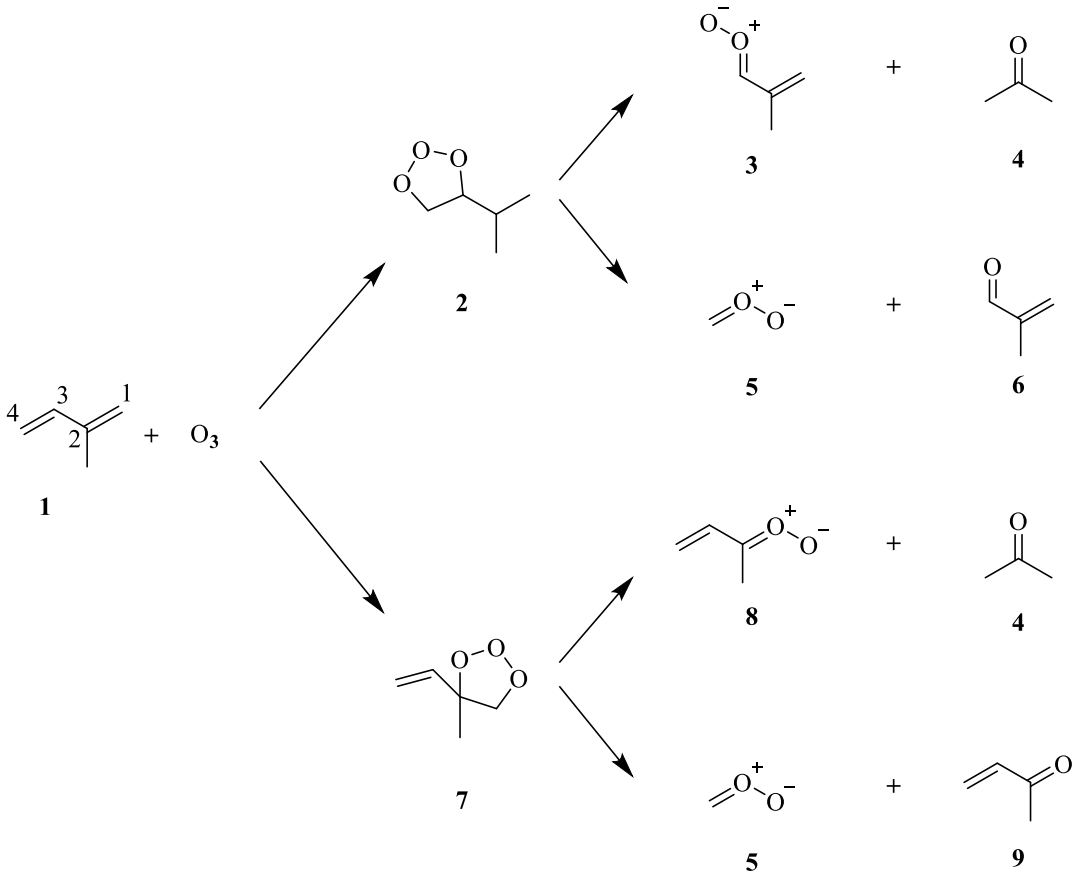

Simpler and saturated Criegee intermediates, such as CH_2OO **5**, CH_3CHOO and $(CH_3)_2COO$, are predicted to have different properties than the four-carbon unsaturated Criegee intermediates like MVK-oxide **8** and MACR-oxide **3**.[21–23] MACR-oxide **3** and MVK-oxide **8** have extended π conjugation involving 6 π electrons that extend over the vinyl and carbonyl group while simpler Criegee intermediates have 4 π electrons across the carbonyl oxide group.[24,25] In addition, each of these four-carbon unsaturated Criegee intermediates have four conformers. The conformers differ from each other in the orientation of the vinyl group with respect to the orientation of the oxygen in the carbonyl oxide group (*syn*- vs *anti*-) and in the relative orientation of the C=C and C=O bonds (*cis* vs. *trans*), as shown in **Figure 1**.[14,15,26] These factors significantly change the electronic properties of MVK-oxide **8** and MACR-oxide **3** from the simpler, saturated Criegee intermediates. The aim of the current study is to characterize the four–carbon unsaturated Criegee intermediate, MACR-oxide **3**, for the first time, using electronic spectroscopy on its first strong $\pi^* \leftarrow \pi$ transition. Since the rate of formation of Criegee intermediates from alkene ozonolysis is much slower than the rate of loss *via* unimolecular and bimolecular

reaction pathways, as observed for **5**,[27,28] an alternative synthesis pathway, using 1,3-diiodo-2-methylprop-1-ene **10** as the precursor, will be employed. This generates sufficient population to characterize MACR-oxide **3** in this study. The method that will be employed in this experiment involves electronic excitation of MACR-oxide **3** on its first strong $\pi^* \leftarrow \pi$ transition coupled with the time of flight mass spectrometry. The resultant experimental spectrum of MACR-oxide **3** has been supported by theoretical calculations.

MACR-oxide **3** can be formed in four distinct conformers that are separated by internal rotation about the C=O bond and the C-C bond, as shown in **Figure 1**. The four conformers are unlikely to interconvert under the present experimental conditions due to substantial barriers for rotation about the C=O and C-C bonds.[26] Each conformer is predicted to have distinct but overlapping electronic spectra associated with the first $\pi^* \leftarrow \pi$ transition.

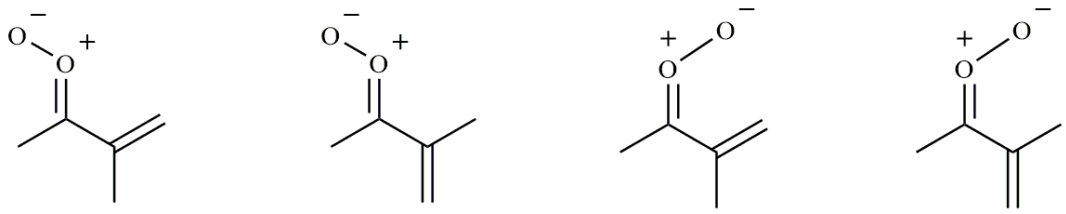

3a **3b** **3c** **3d**

Figure 1. The four conformers of MACR-oxide: **3a** *anti-cis* MACR-oxide; **3b** *anti-trans* MACR-oxide; **3c** *syn-cis* MACR-oxide; **3d** *syn-trans* MACR-oxide, formed upon isoprene ozonolysis.

MACR-oxide **3** has been theoretically predicted to be involved in bimolecular reactions with trace species in the atmosphere.[29–32] The UV-Visible absorption spectroscopy can be employed as a tool for detecting MACR-oxide **3** in laboratory measurements and subsequently studying the rates of bimolecular reactions of this Criegee intermediate with species like water vapor (monomer and dimer), NO_x and SO_2, as adopted previously for the simplest Criegee intermediate CH_2OO **5**.[18,19] These reactions can produce a wide range of products and can lead to the formation of aerosols, which in turn affect the air quality and impact climate.[33] The outcomes of this research can also be extended to investigate the thermal unimolecular and bimolecular decay mechanisms of MACR-oxide **3** under atmospheric conditions.

Materials and Methods

MACR-oxide **3** was generated *in situ* using **Scheme 2** shown in Results and Discussion from the (E)-1,3-diiodo-2-methylprop-1-ene **10** precursor, that was synthesized by Trongsiriwat and Walsh at the University of Pennsylvania. The generation, detection and characterization of MACR-oxide **3** is carried out in a high vacuum chamber that is coupled with a Time-of-Flight Mass Spectrometry set-up. The precursor **10** is introduced into a preheated (Peltier thermoelectric heating module; Laird technology, PC4) pulsed valve (Parker Hannifin Series 9 solenoid valve) at 60 °C (monitored using the Cole Palmer

Type K digital thermometer) along with a 20% O_2/Ar gas mixture at 12 psi. The gas mixture is pulsed into a quartz capillary reactor tube (25 mm in length and 1mm in diameter) and photolysed using a cylindrically focused 248 nm output beam of a KrF excimer laser (Coherent, COMPex 102, 10Hz, 25mJ per pulse). MACR-oxide **3** is formed following the photolysis of the diiodo precursor **10** as described in **Scheme 2** in the Results and Discussions section.

MACR-oxide **3** undergoes supersonic jet expansion and travels about 4 cm downstream to the ion optics region where it is photoionized using 118 nm vacuum ultraviolet (VUV) radiation. The 118 nm light is generated in a phase matched Xe:Ar gas mixture by frequency tripling 355 nm light, which is the third harmonic of a Nd:YAG laser (Continuum Powerlite Series 9010, 10Hz, ~35 mJ/pulse of the 355 nm output beam). The MACR-oxide ion **3** (m/z = 86) formed from this one-photon ionization process travels down a field free region of the Wiley-McLaren linear time of flight mass spectrometer (RM Jordan) and is detected using a pair of microchannel plates. This gives an ionization signal (m/z = 86) that is related to the ground state population of the MACR-oxide **3**.

The UV-Visible depletion of MACR-oxide **3** is induced by introducing UV-Visible radiation using a broadly tunable BBO-OPO (EKSPLA 342NT, 3-5 ns pulse width, 5 cm^{-1} linewidth). The VUV ionization step is delayed by ~50 ns compared to the UV-Visible excitation pulse. The BBO-OPO operates at a repetition rate (5 Hz) of half the frequency of the ionization radiation (10 Hz). Thus, the UV-Visible radiation induces a depletion in the ground state of MACR-oxide **3** on every alternate pulse that the 118 nm radiation ionizes the ground state population of MACR-oxide **3**.

The signal output of the BBO-OPO was used in the 410-500 nm region. In the 315-409 nm region the sum frequency generation (SFG) of the frequency doubled signal + 1064 nm Nd:YAG was used. The typical output power from the BBO-OPO in the 410-500 nm spectral region (signal) is up to 60 mJ/pulse, while the output power in the 315-409 nm (SFG) region is up to 11 mJ/pulse. The OPO wavelength in vacuum was calibrated using a Coherent WaveMaster wavemeter and the power was measured and adjusted using a Gentec TPM/300 power meter. In the 315-395 nm region, the BBO-OPO was stepped at 1 nm increments and it was continuously scanned using a 0.5 nm step size in the 395-500 nm spectral region.

The experimental set up for the depletion method coupled with time of flight mass spectrometry is shown in **Figure 2.** In this experimental set-up, the diiodo alkene precursor **10** along with the 20% O_2/Ar gas mixture at 12 psi backing pressure is introduced via a pulsed valve. The 248 nm radiation from the Excimer photolyses the diiodo precursor preferentially at the $C_{(1)}$-I bond which reacts with the O_2. An iodoalkene peroxy radical **12** is transiently formed with sufficiently high internal energy to rotate about its C-C and C-O bonds. The iodoalkene peroxy radical **12** then loses the iodine atom and forms the four conformers of MACR-oxide **3a, 3b, 3c, 3d**. MACR-oxide **3** formed undergoes supersonic jet expansion which cools MACR-oxide **3** to the ground state of each conformer. MACR-oxide **3** reaches the ion optics assemble ~ 4 cm downstream where it is detected by the 118 nm VUV radiation that ionizes it from its ground state. Depletion in the ground state is induced by irradiating MACR-oxide **3** with UV-Visible radiation from the BBO-OPO ~ 50 ns prior to the 118 nm VUV radiation.

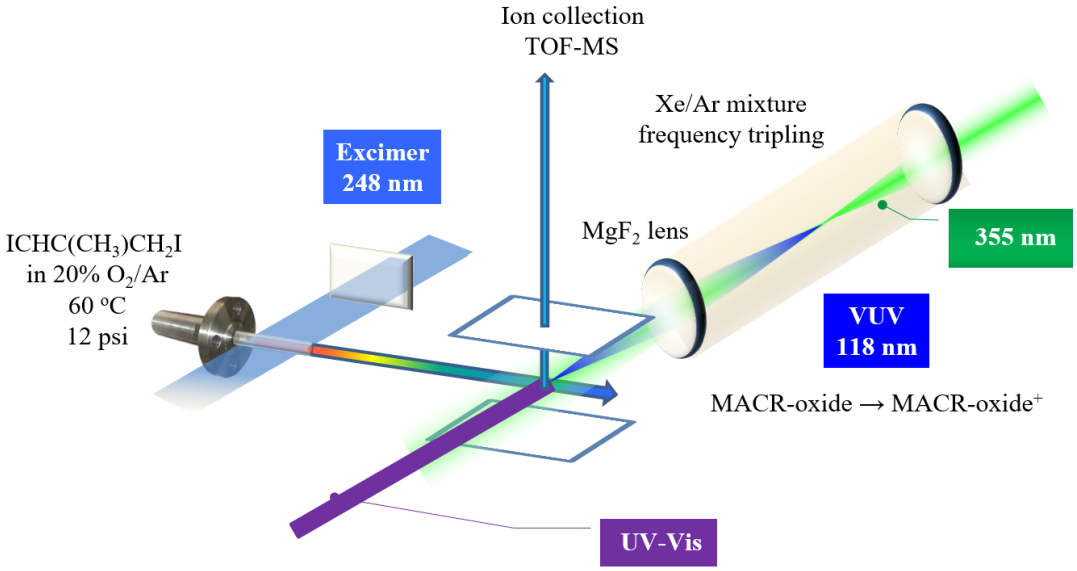

Figure 2. A schematic representation of the TOF-MS set-up in which the electronic spectrum of MACR-oxide **3** was elucidated. The diiodo alkene precursor is introduced in the pulsed valve along with the 20% O_2/Ar carrier gas mixture at 12 psi pressure. The 248 nm radiation (blue) from the Excimer laser photolyzes the diiodo alkene precursor **10** forming MACR-oxide **3** (as shown in Scheme 2). The MACR-oxide **3** undergoes a supersonic jet expansion and reaches the ion optic assembly ~4 cm downstream, where the UV-Visible radiation (purple) is introduced ~50 ns prior to excitation with the 118 nm VUV radiation (green) that ionizes MACR-oxide **3**, and is detected as MACR-oxide$^+$ **3** at m/z = 86 in the TOF-MS.

Results and Discussion

Scheme 2 shows the method used in the laboratory to form MACR-oxide **3**. The (E)-1,3-diiodo-2-methylprop-1-ene precursor **10** is photoyzed at 248 nm to produce a resonantly stabilized monoiodo alkene radical **11**. Photolysis at 248 nm is expected to preferentially dissociate the weaker $C_{(1)}$-I bond to form a mono-iodoalkene radical **11**. The radical formed is resonance stabilized and can react with O_2 to form a transient monoiodoalkene peroxy radical **12.** Due to sufficiently high internal energy of the monoiodo alkene peroxy intermediate **12**, the C-I bond breaks leading to the loss of the Iodine atom. Rotations about the C-C and C-O bond leads to the formation of all four conformers of MACR-oxide **3a, 3b, 3c, 3d**. MACR-oxide **3** is collisionally stabilized in the capillary and subsequently undergoes a supersonic jet expansion into vacuum.

Scheme 2. (E)-1,3-diiodo-2-methylprop-1-ene 10 is photolyzed, producing resonantly stabilized mono-iodo alkene radicals 11, which is followed by O_2 addition to transiently form an iodoalkene peroxy radical 12 and loss of I-atom to form MACR-oxide 3.

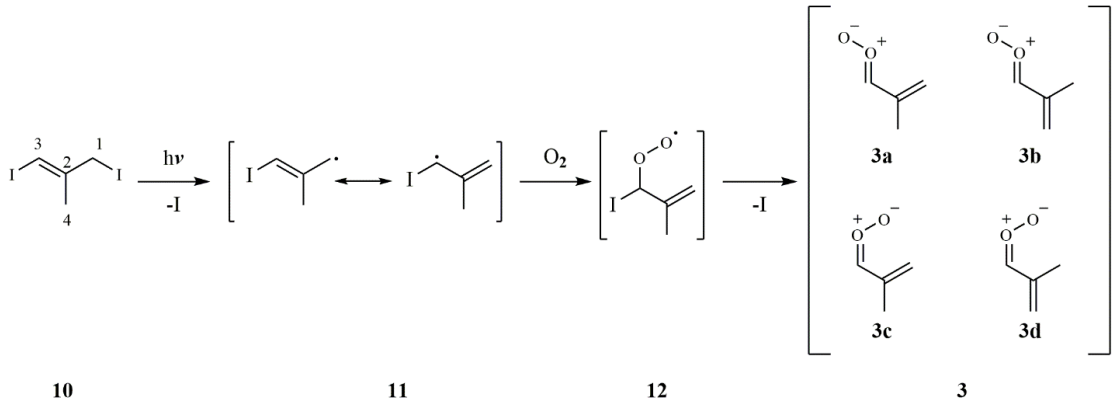

Four conformers of MACR-oxide **3** formed have been predicted to have similar ground states energies but have substantial barriers for interconversion. Stationary point optimizations of MACR-oxide **3** were calculated at the B2PLYP D3/cc-pVTZ level of theory. The energies of each conformer were then evaluated at the CCSD(T)-F12/CBS(TZ-f12,QZ-F12)//B2PLYP-D3/cc-pvtz level of theory. **Table 1** shows the relative ground state energies of the four conformers formed which is in agreement with the trend in ground state energies computed for this system previously.[15]

Table 1. Relative ground state energies (ΔE) for the four conformers of MACR-oxide 3 are calculated at the CCSD(T)-F12/CBS(TZ-f12,QZ-F12)//B2PLYP-D3/cc-pvtz level of theory including Zero Point Energy (ZPE) correction.

MACR-oxide conformer	ΔE / cm^{-1} ($kcal\ mol^{-1}$)
***anti-cis* 3a**	1112 (3.18)
***anti-trans* 3b**	0 (0.00)
***syn-cis* 3c**	317 (0.91)
***syn-trans* 3d**	873 (2.50)

This is the first time that MACR-oxide **3** has been synthetically created, isolated and characterized in the laboratory. Production of the ground state MACR-oxide **3** is demonstrated by the photoionization signal obtained using the 118 nm VUV radiation (10.5 eV) at the parent mass channel at m/z = 86. Based on theoretical calculations, as shown in

Table 2, the 10.5 eV radiation exceeds the ionization energy threshold of all the four conformers of MACR-oxide **3** which are in the range of 8.71- 9.15 eV.

Table 2. Vertical (VIE) and adiabatic (AIE) ionization energies computed at the CCSD(T)-F12/CBS(TZ-F12,QZ-F12)//B2PLYP-D3/cc-pVTZ level of theory for the four conformers of MACR-oxide 3

Conformer	VIE (eV)[b]	AIE (eV)[a]
anti-cis **3a**	8.90	8.77
anti-trans **3b**	8.85	8.73
syn-cis **3c**	9.17	9.01
syn-trans **3d**	8.90	8.78

[a] Including ZPE correction.
[b] Without ZPE correction.

It is calculated that all four conformers of MACR-oxide **3** have similar ionization efficiencies. When subjected to the UV-Visible radiation approximately 50 ns prior to the 118 nm VUV radiation, the MACR-oxide **3** is excited to the $1^1\pi\pi^*$ state from the ground state. This UV-Visible excitation resonant with the $\pi^*\leftarrow\pi$ transition depletes the ground state population of one or more conformers of MACR-oxide **3**. The excitation to the $1^1\pi\pi^*$ state is theoretically predicted to be coupled with repulsive states and hence rapidly dissociates along the O-O bond of MACR-oxide **3**. Once incident with the UV-Visible radiation prior to 118 nm photoionization, only the remainder of the ground state population of MACR-oxide **3** is detected at mass channel m/z = 86. The incident UV-Visible radiation dissociates MACR-oxide **3** in the excited state faster than the time lag of 50 ns between the UV- Visible and 118 nm radiation. This leads to a decrease in the intensity of the signal at mass channel m/z = 86 when MACR-oxide **3** is irradiated with the UV-Visible radiation.

Figure 3 shows the change in the 118 nm induced photoionization signal at the mass channel m/z = 86 due to the $\pi^*\leftarrow\pi$ electronic transition of MACR-oxide **3** caused by the UV-Visible radiation. When excited to the $1^1\pi\pi^*$ state by the UV-Visible radiation, MACR-oxide **3** rapidly dissociates and the 118 nm radiation only detects the remainder of the population of MACR-oxide **3** in the ground state. This gives rise to the depletion of the photoionization signal on the mass channel m/z = 86.

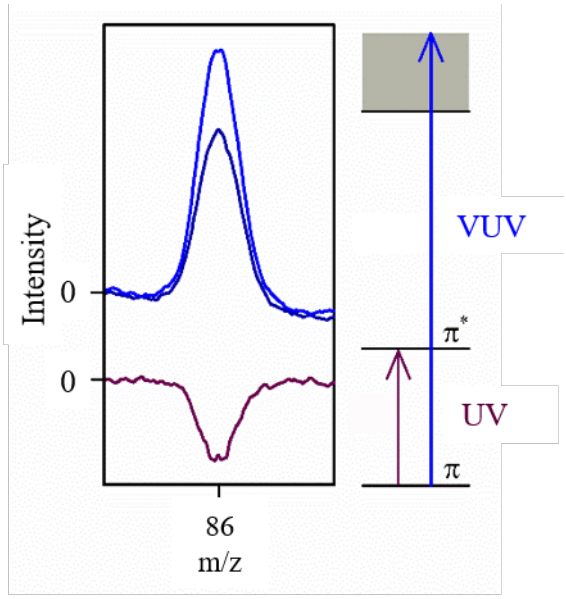

Figure 3. The UV-Visible laser excites the first π*←π transition of MACR-oxide **3**, which causes a depletion in the ground state population of MACR-oxide **3**. The 118 nm VUV radiation (light blue) ionizes MACR-oxide **3** (m/z =86) in its g state and monitors the change in ground state population of MACR-oxide **3** induced by the UV-Visible radiation (dark blue). The difference (magenta trace) between the photoionization signal when the MACR-oxide **3** is irradiated and not irradiated with the UV-Visible, is indicative of the ground state population depletion due to the π*←π electronic transition. The gray region in the ionization scheme represents the ionization continuum of MACR-oxide$^+$ **3**.

An alternating UV-Visible radiation gives the fractional depletion of MACR-oxide **3** as given by **Equation 1**:

$$\% \text{ Depletion} = ((N_0 - N)/N_0) \times 100\% \qquad (1)$$

with N_0 and N being the ground state abundance before and after the UV excitation respectively.

The absorbance σ(λ), at each wavelength λ, can be calculated from these depletion measurements using **Equation 2**:

$$\sigma(\lambda) = -\ln((N_0 - N)/N_0)\Phi(\lambda) \qquad (2)$$

Here, as per **equation (1)**, $(N_0 - N)/N_0$ is the magnitude of the depletion of the ground state and Φ(λ) is the photon flux.

The variation in percentage depletion of MACR-oxide **3** at the mass channel m/z = 86 was monitored over a change in the power of the incident 360 nm UV radiation from the BBO-OPO. The ground state depletion at 360 nm increases with UV power to a

maximum of 35%, as shown in **Figure 4**. A minimum depletion of 2-3% can be reliably measured.

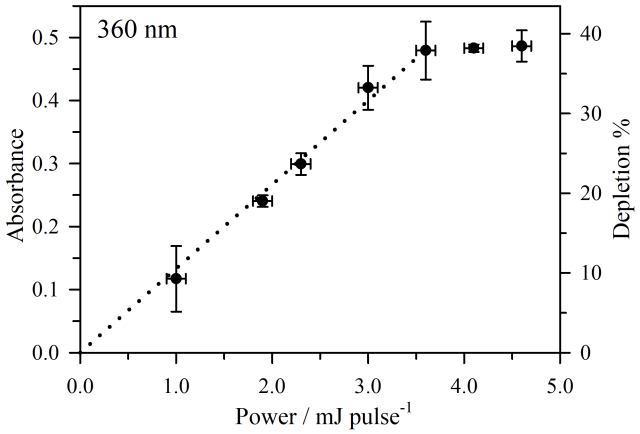

Figure 4. Percentage depletion of the MACR-oxide$^+$ **3** ion mass channel as a function of the power of the incident 360 nm radiation from the BBO OPO. The power dependence plot shows that the absorbance corresponding to the percentage depletions has linear dependence (dashed line) extended up to a power of ~3.6 mJ/pulse of the incoming radiation indicating the one-photon process in this power range. The error bars represent the standard deviation (±1σ) resultant from repeated measurements.

Equation 2 is employed to obtain the absorption cross section based on the ground state population change when the MACR-oxide **3** molecules are subjected to UV-Visible excitation. **Figure 4** shows that the absorbance scales linearly with the OPO power up to 3.6 mJ/pulse at 360 nm. This indicates that the absorption is a one-photon process in this power region. The power of the UV-Visible radiation was maintained at approximately 2.5 mJ/pulse to stay in the linear regime of the power curve.

Figure 5 shows the spectrum for MACR-oxide **3** obtained experimentally. The spectrum obtained is normalized to power. The resultant spectrum is broad and spans the 315-500 nm region. The data points obtained are averages of repeated measurements. The shaded region represents the ±1σ uncertainty in measurements. The spectrum peaks at 380 nm. On the shorter wavelength side, the spectrum initially falls till 340 nm and then starts rising again from 340-315 nm. On the longer wavelength side, the spectrum shows some oscillatory structure. The oscillatory structure is superimposed on a broad Lorentzian profile that peaks at 378.4 nm. This accounts for 90% of the signal in this spectral region. The oscillatory structure accounts for 10% of the signal and are fit to Lorentzians that have local maxima at 416.4 nm, 430.9 nm, and 448.1 nm, respectively. In **Figure 5**, the theoretically computed Vertical Excitation Energy for the four conformers of MACR-oxide **3** at the CASPT2(12,10)/AVDZ level of theory has been plotted with the experimentally obtained spectrum.

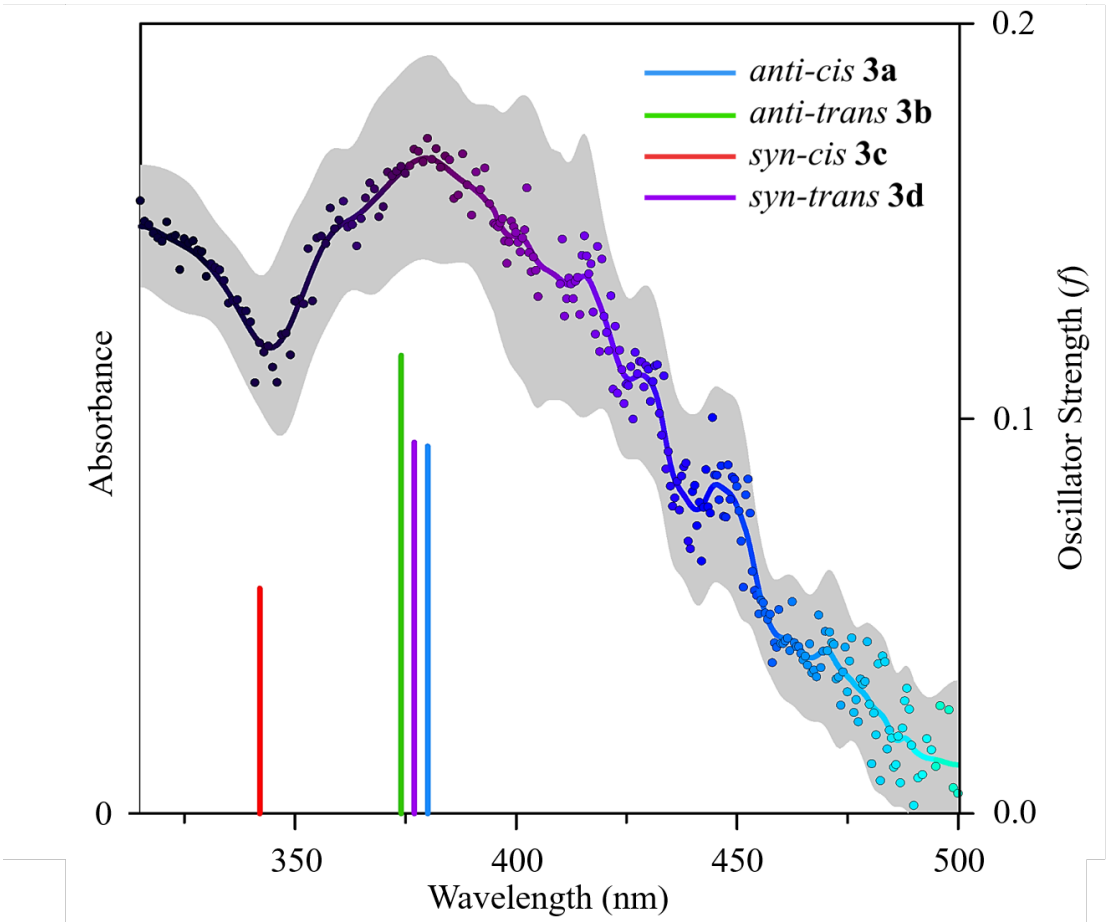

Figure 5. The UV-Visible absorption spectrum of MACR-oxide **3** obtained from the depletion method coupled with the Time-of- Flight Mass Spectrometry. The depletions were recorded using the photoionization signal obtained at the mass channel m/z = 86. The points on the spectrum represent the experimentally obtained UV-Visible spectrum of MACR-oxide **3**. The solid curve is a fit (5 points smooth) and the shaded gray region indicates the uncertainty owing to repeated measurement taken during experiments. The solid bars represent the calculated Vertical excitation energy (VEE) for the first $\pi^*\leftarrow\pi$ electronic transition to the $1^1\,\pi\pi^*$ state of the four conformers of MACR-oxide **3**. The blue, red, green and purple bars represent the VEE for the *anti-cis* **3a**, *anti-trans* **3b**, *syn-cis* **3c**, and *syn-trans* **3d** conformers respectively calculated at the CASPT2(12,10)/AVDZ level of theory.

Previous studies of Criegee intermediates have shown that they have a strong $\pi^*\leftarrow\pi$ electronic transition due to the four π electrons in the zwitterionic carbonyl oxide group ($C{=}O^+O^-$). The oscillator strength is quite large ($f \sim 0.1$)[21–23,34,35]. From previous experimental studies, for the simpler Criegee intermediates like CH_2OO **5**, syn-CH_3CHOO, anti- CH_3CHOO, $(CH_3)_2COO$ and the C_2H_5CHOO, the UV-Visible spectra peaked at 335

nm[21,36,37], 320 nm[38–40], 360 nm[39], 323 nm[23], and 322 nm[23] respectively. However, for the unsaturated, four carbon Criegee intermediate MVK-oxide **8**, the absorption spectrum was shifted to relatively longer wavelengths. **Figure 6** shows the UV-Visible absorption spectra for MACR-oxide **3** and MVK-oxide **8**. MVK-oxide **8** showed an absorption maxima at 388 nm[41]. This can be attributed to the extended π conjugation involving 6 π electrons across the vinyl and carbonyl group. Similar results have been observed in the present study on MACR-oxide **3**. Being isomers of each other, MVK-oxide **8** and MACR-oxide **3** have comparable.

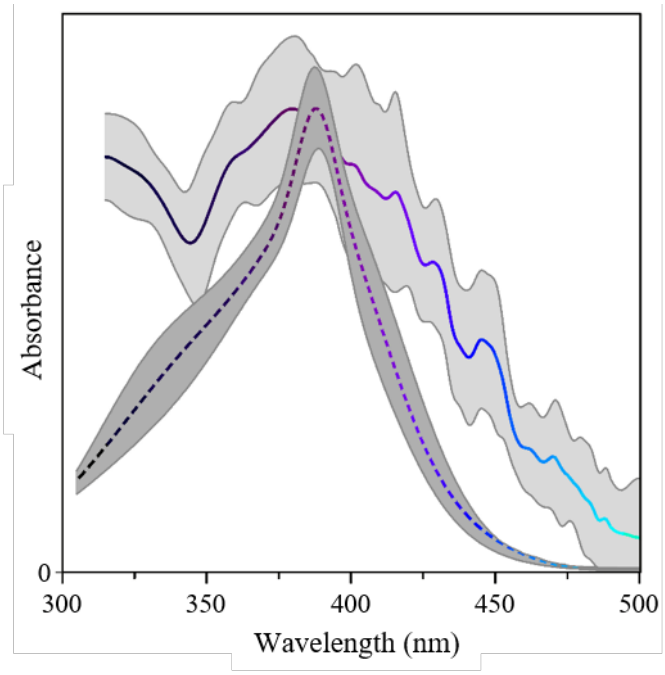

Figure 6. The UV-Visible spectra for MACR-oxide **3** (solid line) and MVK-oxide **8** (dashed line) obtained by the depletions observed at photoionization mass channel m/z = 86. The peak heights of the two spectra have been set equal to one another for comparison. The shaded gray region is the uncertainty calculated as a result of repeated measurement.

Figure 7 shows the UV-Visible absorption spectra of the simpler Criegee intermediates including CH_2OO[37] **5** and $(CH_3)_2COO$[23] in comparison with the spectra obtained for MACR-oxide **3**. **Figure 7** shows that the spectrum for the simpler Criegee intermediates, CH_2OO[37] **5** and $(CH_3)_2COO$[23], peak at lower wavelengths with respect to MACR-oxide **3**. CH_2OO **5** and $(CH_3)_2COO$ have peak maxima at 355 nm and 320 nm respectively while MACR-oxide **3** peaks at 380 nm. This spectral shift is observed since MACR-oxide **3** has extended π conjugation involving 6 π electrons that extend over the vinyl and carbonyl oxide groups, while simpler Criegee intermediates have 4 π electrons across the carbonyl oxide group. An extended π conjugation in the unsaturated Criegee intermediate, MACR-oxide **3**, lowers the transition energy of the molecule with respect to

the transition energy of saturated simpler Criegee intermediates, CH_2OO **5** and $(CH_3)_2COO$.

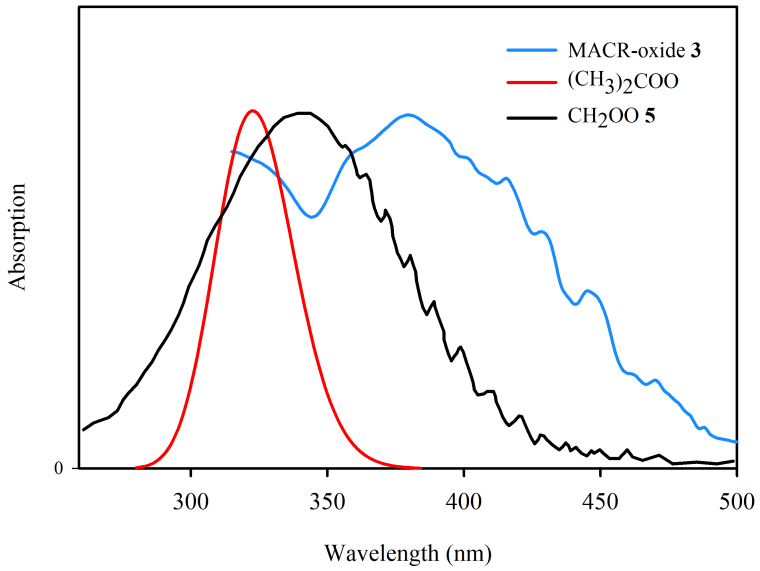

Figure 7. Comparison of the electronic absorption spectra of the simple Criegee intermediates (CH_2OO **5** in black and $(CH_3)_2COO$ in red) with the spectra of conjugated Criegee intermediates (MACR-oxide **3** in blue). The peak maxima of the absorption spectrum of MACR-oxide **3** (380 nm) is shifted to longer wavelengths with respect to the peak maxima of the CH_2OO (355 nm) **5** and $(CH_3)_2COO$ (320 nm) absorption spectra. The peak heights of the three spectra have been adjusted for comparison.

Figure 6 and **Figure 7** clearly show that the UV-Visible absorption spectrum for the unsaturated four-carbon Criegee intermediate, MACR-oxide **3**, is shifted to longer wavelengths with respect to the simpler and smaller Criegee intermediates, CH_2OO **5** and $(CH_3)_2COO$. The oscillatory features observed in the longer wavelength regime of MACR-oxide **3** can be compared to the oscillatory features observed in CH_2OO **5**.

As shown in **Figure 5**, the *syn-cis* MACR-oxide **3** is predicted to have a vertical transition at 342 nm while the other three conformers have vertical transitions in the 374-380 nm range. The spectrum due to the 1^{st} $\pi^*\leftarrow\pi$ electronic transition of MACR-oxide **3** peaks at 380 nm which is in very good agreement with the theoretically predicted vertical excitation energy of the three conformers of MACR-oxide **3** in the 374-380 nm range. This indicates that the spectrum recorded is indeed due to the 1^{st} $\pi^*\leftarrow\pi$ electronic transition of MACR-oxide **3**. The 1^{st} $\pi^*\leftarrow\pi$ electronic transition is quite strong since the ground state depletes significantly. **Table 3** shows the wavelength (λ/nm) associated with the vertical excitation energies (VEE in eV), along with the oscillator strengths (f) theoretically

predicted for the two strong transitions to the $1^1\pi\pi^*$ and $2^1\pi\pi^*$ states for the four conformers of MACR-oxide **3**.

Table 3. Vertical excitation energies (VEE, eV), corresponding wavelengths (λ/nm), and oscillator strengths (*f*) of MACR-oxide 3, starting from the B2PLYP-D3/VTZ optimized geometries, computed at the CASPT2(12,10)/AVDZ level of theory for the $\pi^*\leftarrow\pi$ electronic transition.

MACR-oxide conformer							
anti-cis **3a**		*anti-trans* **3b**		*syn-cis* **3c**		*syn-trans* **3d**	
VEE/eV (λ/nm)	*f*	VEE/eV (λ/nm)	*f*	VEE/eV (λ/nm)	*f*	VEE/eV (λ/nm)	*f*
3.26 (380)	**0.093**	**3.31 (374)**	**0.116**	**3.62 (342)**	**0.057**	**3.29 (377)**	**0.094**
4.07 (304)	**0.083**	**4.31 (288)**	**0.082**	**4.36 (285)**	**0.062**	**5.43 (228)**	**0.110**

The experimental spectrum obtained is very broad which can be attributed to the overlapping electronic spectra of the four conformers that were theoretically calculated. **Figure 8** shows the vertical transitions of the four conformers superimposed with the theoretically predicted spectrum. The vertical excitation energies to the $1^1\pi\pi^*$ and $2^1\pi\pi^*$ states calculated at the CASPT2(12,10)/AVDZ level of theory. The heights of the vertical excitation energy bars correspond to the calculated oscillator strengths of the respective conformers. The theoretical spectrum computed for each conformer of MACR-oxide **3** along with its cumulative spectrum, as shown in **Figure 8**, assumes that all four conformers of MACR-oxide **3** are equally populated. The cumulative spectrum has been rescaled by a factor of 1.5.

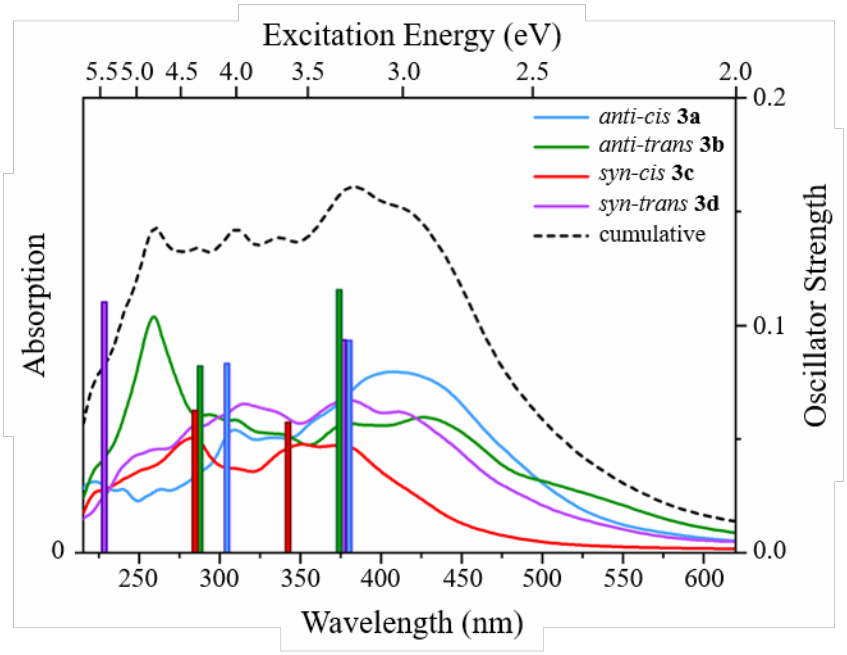

Figure 8. A plot of the theoretically calculated spectra for the four conformers of MACR-oxide **3** compared to the excitation energy and oscillator strengths of each of the conformers for the 1st and 2nd π*←π electronic transition of MACR-oxide **3**. The vertical bars represent the vertical excitation energies to the $1^1\pi\pi^*$ and $2^1\pi\pi^*$ states. Four solid curves in blue, green, red and purple correspond to the calculated spectra obtained for the *anti- cis* **3a**, *anti- trans* **3b**, *syn- cis* **3c**, and *syn- trans* **3d** conformers of MACR-oxide **3** respectively. The black dashed curve represents the cumulative spectrum (rescaled by a factor of 1.5) obtained by summing the spectra of the individual conformers assuming that the four conformers of MACR-oxide **3** are generated in equal concentrations.

On the shorter wavelength region, the rise in the spectrum beyond 340 nm is attributed to the second π*←π electronic transition to the $2^1\pi\pi^*$ state of the four conformers of MACR-oxide **3** based on theoretical calculations. This transition is more likely due to the vinyl group.

In the spectral range 380- 500 nm, the weak oscillatory structures have been fitted to local Lorentzian functions as mentioned previously. These structures could be due to two reasons. The first reason could be that these are the peaks of the overlapped spectra of the four conformers of MACR-oxide **3**. However, since the vertical excitation energies of the four conformers are similar and broad in the spectral domain, it is unlikely that these features are due to the overlap of the electronic spectra of the four conformers.

The other more probable reason for these weak oscillatory structures is attributed to the short-lived vibrational resonances associated with the $1^1\pi\pi^*$ electronic state. Similar oscillatory structure has been observed in the spectra for the simplest Criegee, CH_2OO **5**.[36,37,42,43] These features are known as "resonances" in technical terms. When the wave

function is "on-resonance" the wavefunction appears as a bound state wavefunction that dwells mainly in the potential well, making the probability to find the wave packet, in the said energy state, very high. These oscillatory features are observed when the energy provided to the system is "on–resonance". The spacing between two such oscillatory features is indicative of the energy gap between two consecutive vibrational states in the electronic excited state. The spacing would depend on the energy gap between two states and the shape of the potential energy surface to which the wavefunction has been projected as a result of UV-visible excitation.[44,45] The oscillatory structures observed in CH_2OO **5** were attributed to short-lived resonances originating from closely spaced vibrational structure due to several modes like the O-O stretch and COO bending modes in the excited B^1A' electronic state.

In MACR-oxide **3**, the excitation from ground state to $1^1\pi\pi^*$ state is non-adiabatically coupled with a highly repulsive state. Upon excitation to this state, the coupling of the $1^1\pi\pi^*$ excited state with the $(n/\pi)\sigma^*$ repulsive state forms a quasi- bound state. Resonant excitation of MACR-oxide **3** to the quasi-bound state is what results in the oscillatory features observed in the long wavelength region of the MACR-oxide **3** absorption spectrum. The oscillatory structure in the MACR-oxide **3** spectrum is likely from several vibrational modes including the O-O stretch along the dissociation coordinate from possibly the different conformers of MACR-oxide **3**.

To unravel the distinct contributions of the four conformers of MACR-oxide **3** the UV-Visible absorption spectrum of MACR-oxide **3**, particularly the features in the long wavelength tail region, the individual spectra of the four conformers of MACR-oxide **3** need to be deconvoluted. This would require separation of the conformers and elucidation of their respective contributions to the spectrum.

Other isomers may be created at mass channel m/z = 86 as shown in **Scheme 3**. For example, isomers could be created at the source at mass channel m/z = 86 in this experiment if oxygen adds at the C_1 site of the intermediate **11** formed upon photolysis rather than the C_3 site**.** An isomer of MACR-oxide **3**, namely dioxole **14**, could result as the final product on the mass channel m/z = 86. In addition, MACR-oxide **3** could possibly undergo unimolecular rearrangement pathways to generate other isomers at m/z =86. Dioxole, along with other isomers formed, could contribute to the photoionization signal obtained at mass channel m/z = 86.

Scheme 3. Possible generation of dioxole 14, an isomer of MACR-oxide 3 from (E)-1,3-diiodo-2-methylprop-1-ene 10.

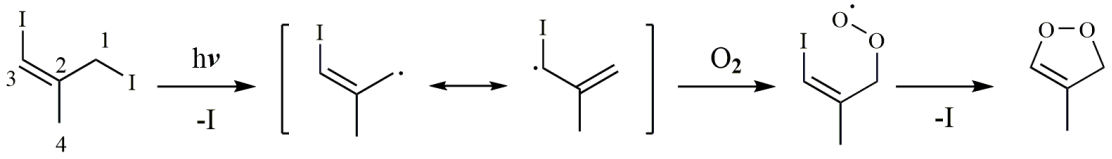

10 **11** **13** **14**

However, these isomers are not predicted to absorb in the UV-Visible region that corresponds to the first $\pi^* \leftarrow \pi$ transition of MACR-oxide **3** and should not contribute to the depletions in the m/z = 86 photoionization signal. However, the possibility of isomers being formed and detected by photoionization on m/z = 86, could result in the underestimation of percentage depletion and resultant cross-section of MACR-oxide in this wavelength region.

To gain a better understanding of the electronic spectroscopy of MACR-oxide **3,** Velocity Map Imaging (VMI) experiments were conducted by coworkers in this laboratory. The VMI experiments show MACR-oxide **3** undergoes photodissociation to MACR X^1A' + O^1D products essentially across its whole UV-vis spectrum. Anisotropic angular distributions of the VMI images indicated that photodissociation of MACR-oxide **3** occurs faster than its rotational period (ca. 100 ps). Rapid dissociation of MACR-oxide **3** in the excited π^* electronic state prevents the subsequent photoionization of the electronically excited MACR-oxide **3**. This assures that the spectrum obtained using the depletion method is equivalent to a direct absorption measurement.

Conclusion

This is the first every laboratory synthesis and direct observation of methacrolein oxide **3** using UV-Visible spectroscopy coupled with the Time of Flight Mass Spectrometry. The electronic spectrum obtained from MACR-oxide **3** in the spectral region 315- 500 nm agrees well with theory for the 1^{st} $\pi^*\leftarrow\pi$ transition. Although theory does not predict the oscillatory structure obtained in the long wavelength region of the MACR-oxide **3** spectrum, the oscillations can be attributed to resonant transitions to the vibrational states in the excited electronic state that have very short lifetimes. These vibrational states can involve several modes in the MACR-oxide **3** molecule including the dissociation coordinate along the O-O bond. The photoexcitation of MACR-oxide **3** in this wavelength region induces a $\pi^*\leftarrow\pi$ transition from ground state to the $1^1\pi\pi^*$ state. The $1^1\pi\pi^*$ couples with repulsive states $(n/\pi)\ \sigma^*$ that cause dissociation of MACR-oxide **3** in the excited state faster than one period of rotation of the MACR-oxide **3** molecule (ca. 100 ps). UV-Visible excitation of MACR-oxide **3** leads to a depletion in the photoionization signal observed 50 ns later using the 118 nm VUV radiation. The depletions obtained can be associated with an absorbance in this wavelength region. The resulting UV-Visible spectrum obtained can be considered equivalent to a direct absorption measurement.

The spectrum obtained for MACR-oxide **3** can have several applications. This spectrum could help understand unimolecular decay pathways, self- reaction and the bimolecular reaction pathways as it provides a direct method to probe the MACR-oxide **3** molecules. MACR- oxide **3** is an important atmospheric species, and is expected to react with other molecules in the atmosphere like water vapor (H_2O and $(H_2O)_2$), NO_x, SO_2, etc. Characterization of MACR-oxide **3** by obtaining its strong UV-Visible absorption spectrum makes it possible to understand and probe the reaction pathways and rates of reaction of MACR-oxide **3** with trace molecules in the atmosphere.

Future Direction

The current study only explores the 1^{st} $\pi^*\leftarrow\pi$ electronic transition to the 1^1 $\pi\pi^*$. The 2^{nd} $\pi^*\leftarrow\pi$ electronic transition to the 2^1 $\pi\pi^*$ state needs to be studied in future studies. An indication of this higher energy transition is observed to be starting in the current spectrum beyond 340 nm on the shorter wavelength side. However, the obstacle in measuring the spectrum beyond 300 nm in the present experimental set up is that the work function of stainless steel is 290 nm. Hence any radiation with energy higher than that will cause the scattered light to generate photoelectrons. Although the experiment is conducted in vacuum conditions (10^{-7} Torr) there are other gas molecules and possibly oil from the diffusion pumps creating the very low-pressure conditions in the vacuum chamber. The photoelectrons created can ionize these molecules present in the chamber to create peaks on other mass channels in the mass spectrum. This causes interference with the mass peak at m/z = 86 making the depletion measurements in the spectral region 210-300 nm not reliable for collecting conclusive results. The solution to this problem is multi fold and involves the possible installation of mass filters to gate only those masses that need to be observed by pulsing the detector with high voltage only at certain times. Other approaches include the use of Brewster's window along with baffles to minimize scattering within the chamber.

Another primary aspect of the experiments that can be conducted in the future includes the separation of the four conformers of MACR-oxide **3**. The relative population of each conformer is unknown in this study but can be investigated in future research. The reaction rates of the *anti*-conformer of MACR-oxide **3** with water, water dimer, and methanol have been calculated to be faster than the *syn*-conformer. [29,30,32] Rate coefficient for the reaction of methanol with the *anti*-conformer and *syn*-conformer of MACR-oxide **3** has been calculated to be on the order of 10^{-13} $cm^3mol^{-1}s^{-1}$ and 10^{-16} $cm^3mol^{-1}s^{-1}$ respectively.[29] In previous experiments conducted in the Lester laboratory, bimolecular reactions have been conducted with organic acids.[46,47] A future project could include the introduction of methanol into the sample line along with the current experimental set up to react away the *anti*-conformer of MACR-oxide **3** faster than the *syn*-conformer since the reaction rate of the *anti*-conformer is predicted to be 1000 times faster than that of the *syn*-conformer of MACR-oxide **3**.[29] This will not only help separate the different conformers but also lead to the separation of the spectra of the different conformers.[48] It will give an idea of the amount of each conformer created in the present experimental set up. Moreover, it will also give an estimate of the contribution of each conformer to the spectrum currently recorded.

References

(1) Müller, J.-F. Geographical Distribution and Seasonal Variation of Surface Emissions and Deposition Velocities of Atmospheric Trace Gases. *J. Geophys. Res.* **1992**, *97* (D4), 3787.

(2) Fehsenfeld, F.; Calvert, J.; Fall, R.; Goldan, P.; Guenther, A. B.; Hewitt, C. N.; Lamb, B.; Liu, S.; Trainer, M.; Westberg, H.; Zimmerman, P. Emissions of Volatile Organic Compounds from Vegetation and the Implications for Atmospheric Chemistry. *Global Biogeochem. Cycles* **1992**, *6* (4), 389–430.

(3) Guenther, A.; Karl, T.; Harley, P.; Wiedinmyer, C.; Palmer, P. I.; Geron, C. Estimates of Global Terrestrial Isoprene Emissions Using MEGAN (Model of Emissions of Gases and Aerosols from Nature). *Atmos. Chem. Phys.* **2006**, *6* (11), 3181–3210.

(4) Sindelarova, K.; Granier, C.; Bouarar, I.; Guenther, A.; Tilmes, S.; Stavrakou, T.; Müller, J.-F.; Kuhn, U.; Stefani, P.; Knorr, W. Global Data Set of Biogenic VOC Emissions Calculated by the MEGAN Model over the Last 30 Years. *Atmos. Chem. Phys* **2014**, *14*, 9317–9341.

(5) Finlayson-Pitts, B. J.; Pitts, J. N. *Chemistry of the Upper and Lower Atmosphere*; Academic Press: San Diego, 2000.

(6) Atkinson, R.; Arey, J. Atmospheric Chemistry of Biogenic Organic Compounds. *Acc. Chem. Res.* **1998**, *31* (9), 574–583.

(7) Atkinson, R.; Arey, J. Atmospheric Degradation of Volatile Organic Compounds. *Chem. Rev.* **2003**, *103* (12), 4605–4638.

(8) Atkinson, R.; Arey, J. Gas-Phase Tropospheric Chemistry of Biogenic Volatile Organic Compounds: A Review. *Atmos. Environ.* **2003**, *37*, 197–219.

(9) Johnson, D.; Marston, G. The Gas-Phase Ozonolysis of Unsaturated Volatile Organic Compounds in the Troposphere. *Chem. Soc. Rev.* **2008**, *37* (4), 699–716.

(10) Welz, O.; Savee, J. D.; Osborn, D. L.; Vasu, S. S.; Percival, C. J.; Shallcross, D. E.; Taatjes, C. A. Direct Kinetic Measurements of Criegee Intermediate (CH_2OO) Formed by Reaction of CH_2I with O_2. *Science* **2012**, *335* (6065), 204–207.

(11) Taatjes, C. A.; Welz, O.; Eskola, A. J.; Savee, J. D.; Scheer, A. M.; Shallcross, D. E.; Rotavera, B.; Lee, E. P. F.; Dyke, J. M.; Mok, D. K. W.; Osborn, D. L.; Percival, C. J. Direct Measurements of Conformer-Dependent Reactivity of the Criegee Intermediate CH3CHOO. *Science (80-.).* **2013**, *340* (6129), 177–180.

(12) Nguyen, T. B.; Tyndall, G. S.; Crounse, J. D.; Teng, A. P.; Bates, K. H.; Schwantes, R. H.; Coggon, M. M.; Zhang, L.; Feiner, P.; Milller, D. O.; Skog, K. M.; Rivera-Rios, J. C.; Dorris, M.; Olson, K. F.; Koss, A.; Wild, R. J.; Brown, S. S.; Goldstein, A. H.; de Gouw, J. A.; Brune, W. H.; Keutsch, F. N.; Seinfeld, J. H.; Wennberg, P. O. Atmospheric Fates of Criegee Intermediates in the Ozonolysis of Isoprene. *Phys. Chem. Chem. Phys.* **2016**, *18* (15), 10241–10254.

(13) Gutbrod, R.; Kraka, E.; Schindler, R. N.; Cremer, D. Kinetic and Theoretical Investigation of the Gas-Phase Ozonolysis of Isoprene: Carbonyl Oxides as an Important Source for OH Radicals in the Atmosphere. *J. Am. Chem. Soc.* **1997**, *119* (31), 7330–7342.

(14) Kuwata, K. T.; Valin, L. C.; Converse, A. D. Quantum Chemical and Master Equation Studies of the Methyl Vinyl Carbonyl Oxides Formed in Isoprene

Ozonolysis. *J. Phys. Chem. A* **2005**, *109* (47), 10710–10725.
(15) Kuwata, K. T.; Valin, L. C. Quantum Chemical and RRKM/Master Equation Studies of Isoprene Ozonolysis: Methacrolein and Methacrolein Oxide. *Chem. Phys. Lett.* **2008**, *451* (4), 186–191.
(16) Aschmann, S. M.; Atkinson, R. *Formation Yields of Methyl Vinyl Ketone and Methacrolein from the Gas-Phase Reaction of 03 with Isoprene*; 1994; Vol. 28.
(17) Mauldin III, R. L.; Berndt, T.; Sipilä, M.; Paasonen, P.; Petäjä, T.; Kim, S.; Kurtén, T.; Stratmann, F.; Kerminen, V. M.; Kulmala, M. A New Atmospherically Relevant Oxidant of Sulphur Dioxide. *Nature* **2012**, *488*, 193–196.
(18) Lewis, T. R.; Blitz, M. A.; Heard, D. E.; Seakins, P. W. Direct Evidence for a Substantive Reaction between the Criegee Intermediate, CH2OO, and the Water Vapour Dimer. *Phys. Chem. Chem. Phys.* **2015**, *17* (7), 4859–4863.
(19) Chao, W.; Hsieh, J.-T.; Chang, C.-H.; Lin, J. J.-M. Direct Kinetic Measurement of the Reaction of the Simplest Criegee Intermediate with Water Vapor. *Science (80-.).* **2015**, *347* (6223), 751–754.
(20) Huang, H.-L.; Chao, W.; Lin, J. J.-M. Kinetics of a Criegee Intermediate That Would Survive High Humidity and May Oxidize Atmospheric SO2. *Proc. Natl. Acad. Sci.* **2015**, *112* (35), 10857–10862.
(21) Beames, J. M.; Liu, F.; Lu, L.; Lester, M. I. Ultraviolet Spectrum and Photochemistry of the Simplest Criegee Intermediate CH2OO. *J. Am. Chem. Soc.* **2012**, *134* (49), 20045–20048.
(22) Beames, J. M.; Liu, F.; Lu, L.; Lester, M. I. UV Spectroscopic Characterization of an Alkyl Substituted Criegee Intermediate CH3CHOO. *J. Chem. Phys.* **2013**, *138* (24), 244307.
(23) Liu, F.; Beames, J. M.; Green, A. M.; Lester, M. I. UV Spectroscopic Characterization of Dimethyl- and Ethyl-Substituted Carbonyl Oxides. *J. Phys. Chem. A* **2014**, *118* (12), 2298–2306.
(24) Yin, C.; Takahashi, K. How Does Substitution Affect the Unimolecular Reaction Rates of Criegee Intermediates? *Phys. Chem. Chem. Phys.* **2017**, *19* (19), 12075–12084.
(25) Yin, C.; Takahashi, K. Effect of Unsaturated Substituents in the Reaction of Criegee Intermediates with Water Vapor. *Phys. Chem. Chem. Phys.* **2018**, *20* (30), 20217–20227.
(26) Barber, V. P.; Pandit, S.; Green, A. M.; Trongsiriwat, N.; Walsh, P. J.; Klippenstein, S. R.; Lester, M. I. Four Carbon Criegee Intermediate from Isoprene Ozonolysis: Methyl Vinyl Ketone Oxide Synthesis, Infrared Spectrum, and OH Production. *J. Am. Chem. Soc.* **2018**, *140* (34), 10866–10880.
(27) Womack, C. C.; Martin-Drumel, M.-A.; Brown, G. G.; Field, R. W.; Mccarthy, M. C. Observation of the Simplest Criegee Intermediate CH 2 OO in the Gas-Phase Ozonolysis of Ethylene. https://doi.org/10.1126/sciadv.1400105.
(28) Taatjes, C. A.; Shallcross, D. E.; Percival, C. J. Intermediates Just Want to React. *Nat. Chem.* **2014**, *6* (6), 461–462. https://doi.org/10.1038/nchem.1966.
(29) Watson, N. A. I.; Black, J. A.; Stonelake, T. M.; Knowles, P. J.; Beames, J. M. An Extended Computational Study of Criegee Intermediate–Alcohol Reactions. *J. Phys. Chem. A* **2019**, *123* (1), 218–229.
(30) Vereecken, L.; Novelli, A.; Taraborrelli, D. Unimolecular Decay Strongly Limits

the Atmospheric Impact of Criegee Intermediates. *Phys. Chem. Chem. Phys.* **2017**, *19* (47), 31599–31612.
(31) Anglada, J. M.; Gonzalez, J.; Torrent-Sucarrat, M. Effects of the Substituents on the Reactivity of Carbonyl Oxides. A Theoretical Study on the Reaction of Substituted Carbonyl Oxides with Water. *Phys. Chem. Chem. Phys.* **2011**, *13* (28), 13034–13045.
(32) Anglada, J. M.; Sole, A. Impact of the Water Dimer on the Atmospheric Reactivity of Carbonyl Oxides. *Phys. Chem. Chem. Phys.* **2016**, *18* (26), 17698–17712.
(33) Mentel, T. F.; Springer, M.; Ehn, M.; Kleist, E.; Pullinen, I.; Kurtén, T.; Rissanen, M.; Wahner, A.; Wildt, J. Formation of Highly Oxidized Multifunctional Compounds: Autoxidation of Peroxy Radicals Formed in the Ozonolysis of Alkenes – Deduced from Structure–Product Relationships. *Atmos. Chem. Phys.* **2015**, *15* (12), 6745–6765.
(34) Aplincourt, P.; Anglada, J. M. Theoretical Studies on Isoprene Ozonolysis under Tropospheric Conditions. 1. Reaction of Substituted Carbonyl Oxides with Water. *J. Phys. Chem. A* **2003**, *107* (30), 5798–5811.
(35) Samanta, K.; Beames, J. M.; Lester, M. I.; Subotnik, J. E. Quantum Dynamical Investigation of the Simplest Criegee Intermediate CH2OO and Its O-O Photodissociation Channels. *J. Chem. Phys.* **2014**, *141* (13), 134303.
(36) Sheps, L. Absolute Ultraviolet Absorption Spectrum of a Criegee Intermediate CH 2 OO. *J. Phys. Chem. Lett.* **2013**, *4* (24), 4201–4205.
(37) Ting, W.-L.; Chen, Y.-H.; Chao, W.; Smith, M. C.; Lin, J. J.-M. The UV Absorption Spectrum of the Simplest Criegee Intermediate CH2OO. *Phys. Chem. Chem. Phys.* **2014**, *16*, 10438–10443.
(38) Meng, Q.; Meyer, H. D. A Full-Dimensional Multilayer Multiconfiguration Time-Dependent Hartree Study on the Ultraviolet Absorption Spectrum of Formaldehyde Oxide. *J. Chem. Phys.* **2014**, *141* (12), 124309.
(39) Sheps, L.; Scully, A. M.; Au, K. UV Absorption Probing of the Conformer-Dependent Reactivity of a Criegee Intermediate CH3CHOO. *Phys. Chem. Chem. Phys.* **2014**, *16* (48), 26701–26706.
(40) Smith, M. C.; Ting, W. L.; Chang, C. H.; Takahashi, K.; Boering, K. A.; Lin, J. J. UV Absorption Spectrum of the C2 Criegee Intermediate CH3CHOO. *J. Chem. Phys.* **2014**, *141* (7), 74302.
(41) Vansco, M. F.; Marchetti, B.; Lester, M. I. Electronic Spectroscopy of Methyl Vinyl Ketone Oxide: A Four-Carbon Unsaturated Criegee Intermediate from Isoprene Ozonolysis. *J. Chem. Phys.* **2018**, *149* (24), 244309.
(42) Foreman, E. S.; Kapnas, K. M.; Jou, Y.; Kalinowski, J.; Feng, D.; Gerber, B. R.; Murray, C. High Resolution Absolute Absorption Cross Sections of the B1A'-X1A' Transition of the CH2OO Biradical. *Phys. Chem. Chem. Phys.* **2015**, *17*, 32539–32546.
(43) Vansco, M. F.; Li, H.; Lester, M. I. Prompt Release of O (1)D Products upon UV Excitation of CH2OO Criegee Intermediates. *J. Chem. Phys.* **2017**, *147* (1), 13907.
(44) Kuklin, V.I., Kransnopol'sky, V.M., Horácek, J. *Theory of Resonances: Principles and Applications*; Prof. Ing. Jiri Formanek, D., Ed.; Kluwer Academic Publishers, 1989.
(45) Schinke, R.; Keller, H.-M.; Stumpf, M.; Dobbyn, A. J. Vibrational Resonances in

Molecular Photodissociation: From State-Specific to Statistical Behaviour. *J. Phys. B At. Mol. Opt. Phys.* **1995**, *28* (15), 3081–3111.
(46) Welz, O.; Eskola, A. J.; Sheps, L.; Rotavera, B.; Savee, J. D.; Scheer, A. M.; Osborn, D. L.; Lowe, D.; Murray Booth, A.; Xiao, P.; Khan, A. H. M.; Percival, C. J.; Shallcross, D. E.; Taatjes, C. A. Rate Coefficients of C1 and C2 Criegee Intermediate Reactions with Formic and Acetic Acid Near the Collision Limit: Direct Kinetics Measurements and Atmospheric Implications. *Angew. Chemie Int. Ed.* **2014**, *53* (18), 4547–4550.
(47) Liu, F.; Fang, Y.; Kumar, M.; Thompson, W. H.; Lester, M. I. Direct Observation of Vinyl Hydroperoxide. *Phys. Chem. Chem. Phys.* **2015**, *17* (32), 20490–20494.
(48) Khan, M. A. H.; Percival, C. J.; Caravan, R. L.; Taatjes, C. A.; Shallcross, D. E. Criegee Intermediates and Their Impacts on the Troposphere. *Environ. Sci. Process. Impacts* **2018**, *20* (3), 437–453.
(49) Bernath, P. F. *Spectra of Atoms and Molecules*, 2nd Edition.; Oxford University Press: New York, 2005.
(50) Smalley, R. E.; Wharton, L.; Levy, D. H. *Spectroscopy with Supersonic Jets 139 Molecular Optical Spectroscopy with Supersonic Beams and Jets*; 1977; Vol. 10.
(51) Aidong, J.; Fen, C.; Qi, L.; Zusheng, C.; Yong, Z. Flux Growth of Large Single Crystals of Low Temperature Phase Barium Metaborate. *J. Cryst. Growth* **1986**, *79* (1–3), 963–969.
(52) Harris, S. E. Tunable Optical Parametric Oscillators. *Proc. IEEE* **1969**, *57* (12), 2096–2113.
(53) Katzenstein, H. S.; Friedland, S. S. New Time-of-Flight Mass Spectrometer. *Rev. Sci. Instrum.* **1955**, *26* (4), 324–327.
(54) Ionization Energy, Ei. In *IUPAC Compendium of Chemical Terminology*; IUPAC: Research Triagle Park, NC.
(55) CCCBDB Notes on Ionization Energies https://cccbdb.nist.gov/adiabatic.asp (accessed Mar 24, 2019).
(56) Heisenberg, W. Über Den Anschaulichen Inhalt Der Quantentheoretischen Kinematik Und Mechanik. *Zeitschrift für Phys.* **1927**, *43* (3–4), 172–198.
(57) Sciama, D. W. The Physical Significance of the Vacuum State of a Quantum Field. 1991.

Appendix 1. Terms and Definition

UV Spectroscopy: It is a method which uses electromagnetic radiation in the Ultraviolet Region for light-matter interaction to excite molecules from the ground electronic state to an electronically excited state.[49]

Supersonic expansion: A supersonic expansion occurs when a high-pressure gas is expanded through a small orifice into vacuum such that the gas undergoes adiabatic expansion leading to a fall in the temperature of the gas. Since the gas is actually a mixture of buffer gas with a small percentage of the molecule that is to be studied, the molecules undergo many, many collisions with the buffer gas. In these collisions, the sample molecules acquire the temperature of the abundant carrier gas and cools down, losing most of its vibrational and rotational energy. This situation is ideal for doing spectroscopy because it greatly reduces the number of transitions the molecule can undergo.[50]

BBO OPO: Barium borate is an inorganic compound, a borate of barium with a chemical formula BaB_2O_4 or $Ba(BO_2)_2$. BBO crystals are bifringent and have non-linear properties. It is a Second Harmonic Generating crystal and has a high SHG coefficient. It also has a wide transparent waveband, low grounserature coefficient of refractive index, broad phase-matched range, good chemical stability, high damage threshold, and is not deliquescent.[51] An optical parametric oscillator (OPO) uses the principle of second-order nonlinear optical interaction to convert an input laser wave (called "pump") with frequency ω_p to two output waves of lower frequency, "signal" (ω_s) and "idler" (ω_i) by means of second-order nonlinear optical interaction. The OPO consists of two major components, namely the optical resonator and the non-linear optical crystals. The optical resonator facilitates optical oscillations of the signal and/or idler waves while the crystals induce optical interaction of the pump, signal and idler waves to promote parametric amplification of the signal and idler waves and deamplifies the pump wave. The final output from an OPO depends on the gain due to the resonant oscillations and losses due to these oscillations and other optical components in the OPO.[52] OPOs that use BBO crystals for parametric generation of radiation are called BBO OPOs.

Time-Of-Flight Mass Spectrometry (TOF-MS): Time-of-flight mass spectrometry (TOFMS) is a method in which a molecular ion of mass –by- charge ratio (m/z) approaches the detector with different velocities in a vacuum chamber. Greater the m/z ratio, the longer will it take for the ion to reach the detector with respect to other ions with lower m/z ratio in the vacuum chamber when accelerated through the same potential. The time that it subsequently takes for the ion to reach a detector at a known distance is measured. From this ratio and previously known experimental parameters the ion can be identified based on its time of arrival at the detector.[53]

Vertical Ionization Energy (VIE): VIE refers to the energy required by a molecule in the ground state to transition to the molecular ion without any change in its geometry.

This implies that the transition may have been from the lowest vibrational state of the molecule but it may not be necessarily excited to the lowest vibrational state of the molecular ion. The value of VIE is governed by the Franck- Condon principle.[54,55]

Adiabatic Ionization Energy (AIE): AIE refers to the energy required by a neutral molecule to get ionized from its lowest vibrational state in the ground state to the lowest vibrational state of the molecular ion. The specific equilibrium geometry is independent of this value.[54,55]

Zero Point Energy (ZPE): The lowest energy of a quantum mechanical system cannot be zero. Even in the ground state, the wavefunction is bound to undergo fluctuations. In order to satisfy the Heisenberg's uncertainty principle, the lowest energy of a system cannot be the lowest point of the potential energy surface. This gives rise to the lowest possible energy of a quantum mechanical system in the ground state which is termed as Zero Point Energy.[56,57]